J. Mech. Phys. Solids Vol. 38, No. 5, pp. 681–699, 1990.
Printed in Great Britain.

0022–5096/90 $3.00 + 0.00

LOCALIZATION OF PLASTIC DEFORMATION IN SHEAR DUE TO MICROCRACKS

P. M. ANDERSON,† N. A. FLECK‡ and K. L. JOHNSON‡

†Department of Materials Science and Engineering, The Ohio State University, Columbus, OH 43210-1179, U.S.A.; ‡Department of Engineering, University of Cambridge, Trumpington Street, Cambridge CB2 1PZ, U.K.

(*Received* 15 *August* 1989)

ABSTRACT

A CONSTITUTIVE relation for simple shear of an elastic–plastic material containing a periodic array of cracks is developed. The relation is based on finite element analysis and slip-line field solutions for interacting cracks in simple shear. Typical shear stress–strain curves display a peak in the nominal shear stress due to competition between strain hardening of the matrix and material softening due to rotation and stretching of cracks with deformation. The effect of nonuniform crack distributions on localization behavior is studied by determining the critical conditions for which the shear strain in a band of cracks becomes unbounded relative to that in the surrounding, uncracked material. The results show that the strain to localization depends strongly on the ratio of crack length to crack spacing, crack orientation, crack-face friction and matrix hardening. The results are helpful to understanding shear localization under confining pressures, where voids adopt a crack-like morphology.

1. INTRODUCTION

FAILURE of nominally ductile materials is sometimes associated with the onset of localized plastic deformation along narrow shear bands. Once formed, shear bands signify imminent failure by the rapid nucleation, growth and coalescence of voids and cracks within the band. Under increasing confining pressure, failure may be delayed due to void collapse, increasing crack-face friction or suppression of void nucleation. In the limit of sufficiently large confining pressure, shearing of the band eventually produces necking of the specimen to a point (e.g. TEIRLINK *et al.*, 1988).

This work addresses the onset of shear banding under conditions where local stresses at inclusion–matrix interfaces produce debonding into a void, but where the macroscopic pressure and shearing loads produce stretching and collapse of voids into cracks. Examples are a rolled, low carbon steel loaded in torsion (Fig. 1), and sliding frictional contact geometries, where shear bands in the highly deformed near-surface layer are thought to produce wear flakes (SUH, 1986).

In this paper, an elastic–plastic constitutive relation is developed for a band of cracks in shear. The band softens at large strains by the stretching and rotation of the cracks. Crack tip growth associated with the strain singularity at the crack tip is neglected. The development adopts an idealized, two-dimensional periodic cell model containing a crack, for which the ratio of crack length to crack spacing and crack orientation angle are the internal damage variables. Slip-line field techniques and finite

element analysis are used to obtain the nominal shear stress at which the band reaches limit load, as a function of the current damage, confining pressure, crack-face friction, and flow stress of the perfectly plastic matrix material. These solutions also suggest how existing damage may evolve with continued shearing. Consistency and equivalence of plastic work are used to produce an approximate incremental shear stress–strain relation for the band when the matrix material exhibits work-hardening.

This constitutive relation complements a popular relation developed for voided materials by GURSON (1977, 1975). In that analysis, an isotropic hardening law using void volume fraction as a scalar damage parameter is developed from an approximate yield condition for a thick spherical shell volume element. The Gurson model is most applicable to stress states with a large tensile hydrostatic component since a spherical void *shape* is more likely to be maintained for such loadings. The present analysis considers the effect of void shape by studying the limiting case of sliding (mode II) cracks. For simple shear of a voided material with an incompressible matrix, the Gurson model predicts no mechanical softening due to damage evolution, whereas the present analysis does.

In order to evaluate the effect of nonuniform crack distributions on localization behavior, a bifurcation analysis as developed by YAMAMOTO (1978) is used. Here, an initial band of cracked material characterized by a crack density, crack orientation, and a constitutive law in shear as described earlier is embedded in an uncracked matrix. The initial imperfection is assumed to exist from nonhomogeneous nucleation during prior deformation or processing. Critical conditions for which the strain increment in the band becomes infinite while that outside the band remains finite are determined as a function of initial crack size and spacing, crack orientation, and matrix work-hardening. The estimates of localization strain in simple shear are regarded as an upper bound since in the present analysis, the imperfection band is restricted to remain parallel to the direction of simple shear.

2. THE YIELD LOCUS FOR AN ARRAY OF CRACKS IN SHEAR

Observations of nominally ductile materials in shear, as shown in Fig. 1, suggest possible localization of deformation in a shear band of cracks. An idealized 2-D model of such a band is depicted as a periodic array of cracks as shown in Fig. 2(a). The cracks are assumed to have uniform length $2a$, spacing $2L$ and inclination angle θ, as might be expected when crack nucleation sites are evenly spaced in a material under uniform loading. In order to determine the mechanical response of a shear band in terms of a nominal shear stress τ and shear strain γ across the band, a yield locus in shear is first obtained. Here, the matrix surrounding the cracks is assumed to be perfectly plastic with a yield stress in shear equal to k, and the critical value of τ at which the band of cracks collapses is determined by using finite element methods and slip-line field techniques.

Finite element study of shear band collapse

Finite element analyses of the crack array were employed to determine the stress and deformation field between interacting cracks in simple shear, and to supplement

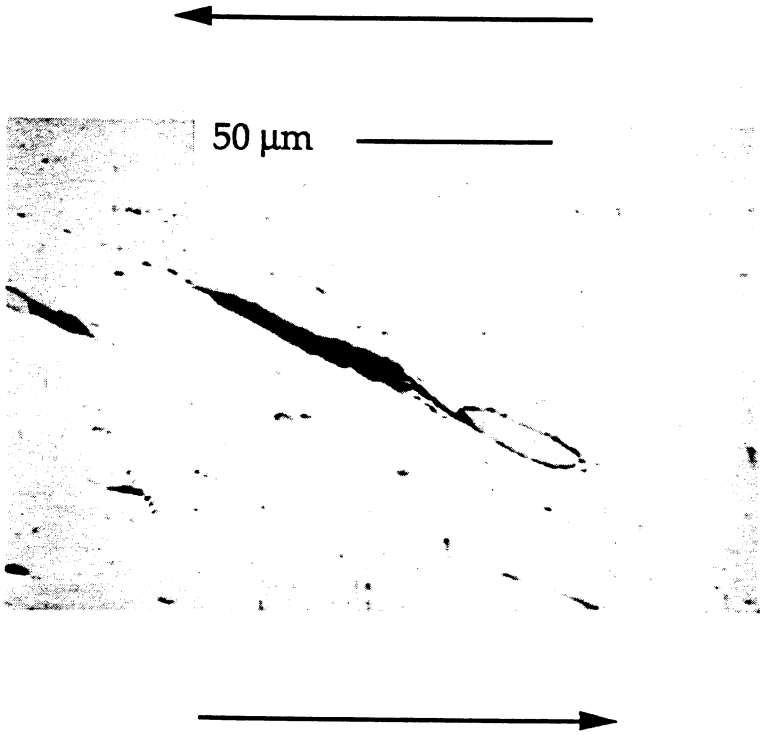

FIG. 1. Nucleation and growth of cracks at MnS particles, observed in a rolled, low carbon steel loaded in torsion (KAPOOR, 1987). The arrows show the direction of shear deformation.

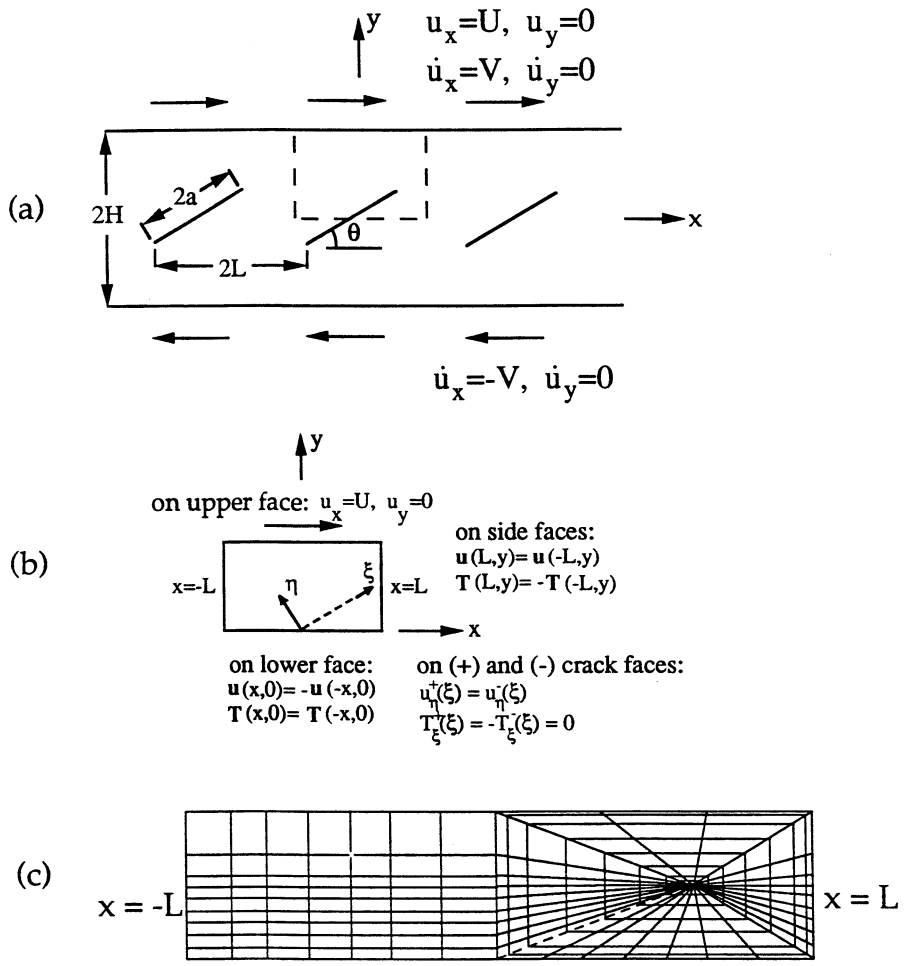

FIG. 2. (a) Geometry of an idealized crack array loaded in simple shear, in which the dotted region depicts a periodic half-cell. (b) Boundary conditions for one-half of a frictionless crack cell employed in the finite element analysis. The crack is shown by a dotted line. (c) A typical finite element mesh used for the half-cell geometry depicted in (b).

slip-line field solutions to be discussed. The periodic structure of the band in the x-direction and two-fold rotational symmetry about the midpoint of a crack permits analysis of only one-half of a crack cell as shown in Fig. 2(b). In particular, displacements $\mathbf{u}$ and tractions $\mathbf{T}$ along the side faces, $x = L$ and $x = -L$, of the half-cell must satisfy the periodic boundary conditions that $\mathbf{u}(L, y) = \mathbf{u}(-L, y)$ and $\mathbf{T}(L, y) = -\mathbf{T}(-L, y)$. The two-fold rotational symmetry about the point $x = 0, y = 0$ requires that displacements and tractions on the right and left halves of the lower face, $y = 0$, are related by $\mathbf{u}(x, 0) = -\mathbf{u}(-x, 0)$ and $\mathbf{T}(x, 0) = \mathbf{T}(-x, 0)$. The final condition that the band deform nominally by simple shear requires that the vertical displacement u_y on the upper face equals zero, while the horizontal displacement u_x on that face is applied. Rigid translation of the half-cell is prevented by imposing $u_x(-L, 0) = u_x(L, 0) = 0$, consistent with the periodicity, two-fold rotational symmetry and simple shear deformation of the half-cell. Crack face conditions consistent with a freely sliding, closed crack were obtained by setting the normal component of

displacement across the crack to be continuous and the tangential component of traction on the crack surfaces to be zero.

A typical finite element mesh of a half-cell with prescribed angle θ and crack length to spacing ratio a/L is shown in Fig. 2(c) and contains approximately 300 4-noded plane strain constant dilatation elements. The locations of the nodes on the cell boundary and crack surfaces must satisfy the proper periodic and two-fold rotational symmetry conditions in order to enforce the boundary conditions described above. Elements were concentrated at the crack tip to better model the singularity in strain. Further, elements were concentrated in a band given by the projected height of the crack. The total height of the cell was one and one-half to two times the projected height of the crack to allow for more widespread plastic flow.

The perfectly plastic property of the matrix was used to help produce a well-defined collapse load, unlike that for a work-hardening matrix. The corresponding numerical problems associated with the study of incompressible rigid–plastic flow were alleviated by including an elastic portion in the matrix material response and by employing four-noded constant dilatation elements as suggested by NAGTEGAAL *et al.* (1974). The isotropic elastic behavior was described by an elastic shear modulus G equal to 1000 times the yield stress k in shear, and Poisson's ratio $\nu = 0.45$.

Finite element calculations were performed for various crack sizes and orientations, but are presented here for $a/L = 1/3$ and $2/3$, and θ in the range 0 to 45°. The analysis employed a general purpose finite element program MARC (1983); analysis for a given crack orientation angle and crack size to spacing ratio used between five to fifteen minutes of CPU on an IBM 4341 mainframe computer.

The finite element calculations furnish for a given a/L and θ the nominal shear traction τ as a function of the applied nominal shear strain $\gamma(=u_x/H)$. Figure 3 displays some typical features, and shows the approximately linear increase in τ with γ, which occurs as a plastic zone grows from each crack tip but remains well confined by surrounding elastic material. When γ reaches approximately the yield strain γ_y in

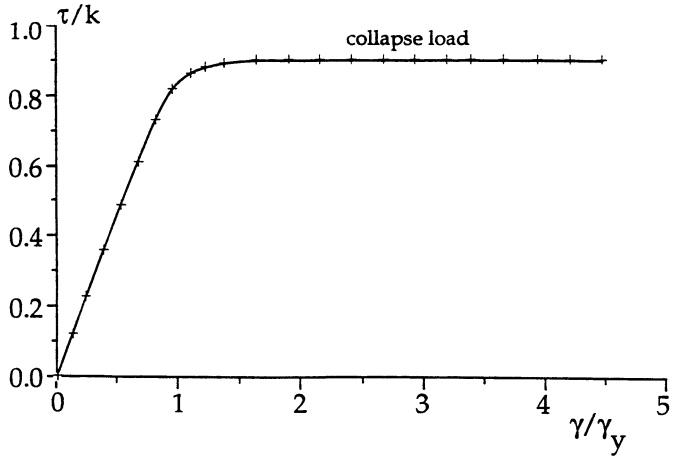

FIG. 3. Finite element results showing a typical plot of nominal shear stress vs nominal shear strain for the idealized array of cracks. The shear stress and strain are normalized, respectively, by the yield stress and strain of the matrix in shear.

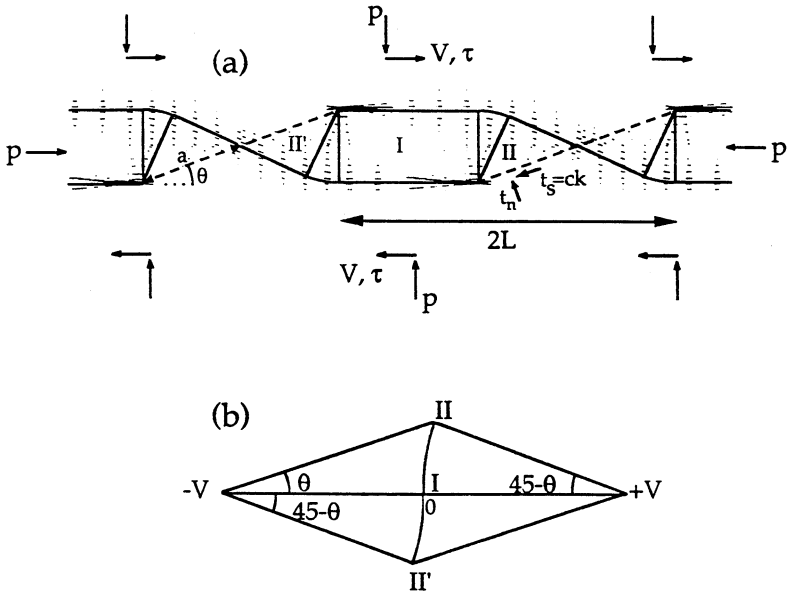

FIG. 4. (a) Predictions by finite element analysis of the local slip-line directions for a frictionless crack array in shear, as shown by short line segments oriented along a direction of principal shear and with length linearly proportional to the magnitude of principal shear. The solid black lines show the corresponding complete slip-line field solution. The dotted lines depict freely sliding cracks with $\theta \approx 20.7°$ and $a/L = 2/3$. (b) The hodograph to the slip-line field in (a).

shear, τ abruptly levels off to a collapse load less than the yield stress k in shear. The collapse load corresponds to the overlapping of plastic zones from crack tips in two adjacent cells and the formation of a fully plastic ligament between the cracks. Deformation was continued to values of several times γ/γ_y to establish a well-defined collapse load plateau and to insure that plastic strain increments were considerably larger than elastic strain increments in yielded regions of the crack array.

The finite element solutions described were used to help motivate slip-line field solutions for crack arrays in a rigid, perfectly plastic matrix as discussed in the next section. Figure 4(a) provides a spatial plot of the local directions of principal shear, based on the final plastic strain increments at the end of a loading history. These line segments have length directly proportional to the magnitude of principal shear strain, and show the local orientation for which the strain increment consists of pure shear and the stress state consists of pure shear plus hydrostatic pressure. Superimposed in Fig. 4(a) is the actual slip-line field. The finite element solution compares favorably, although it is clear that lines of shear discontinuity are substantially broadened. In general, shear discontinuities can not be modelled very well, even when the density of finite elements is increased substantially in such regions. This is due in part to the elastic component of the matrix response. However, as will be shown in the next section, the finite element method accurately predicts collapse loads of the crack array and complements the slip-line field approach. In addition, more accurate descriptions of matrix materials which incorporate work-hardening, for instance, may be included directly in the finite element analysis.

Slip-line fields of crack arrays

The finite element solutions discussed helped to motivate slip-line field solutions for crack arrays in shear. With the exception of geometries with crack orientation angle equal to 0 or 90° (NAGPAL *et al.*, 1972), the fields presented here have not, to the authors' knowledge, appeared in the literature.

The slip-line fields for the shear crack geometry shown in Fig. 2(a) degenerate into simple forms at discrete angles between 0 and 45° inclusive given by

$$\theta_n = \sin^{-1}\left(\frac{n}{n+1}\sqrt{\frac{1-c}{2}}\right), \tag{2.1}$$

where n is a non-negative integer, and c relates the uniform frictional shear stress t_s on the crack surfaces to the yield stress k in shear of the rigid, perfectly plastic matrix by

$$t_s = ck. \tag{2.2}$$

Figures 4 and 5 show the essential features of the discrete angle slip-line fields, in which the ligament between the cracks is divided horizontally into n rigid, sliding rectangular blocks ($n = 1$ in Fig. 4, $n = 3$ in Fig. 5), and each crack surface is divided equally among $n+1$ rigid regions. The solution predicts each crack to kink, due to the lines of velocity discontinuity which intersect the crack surface. In actual materials which work-harden, these lines would broaden substantially and most likely produce rotated and curved rather than kinked cracks.

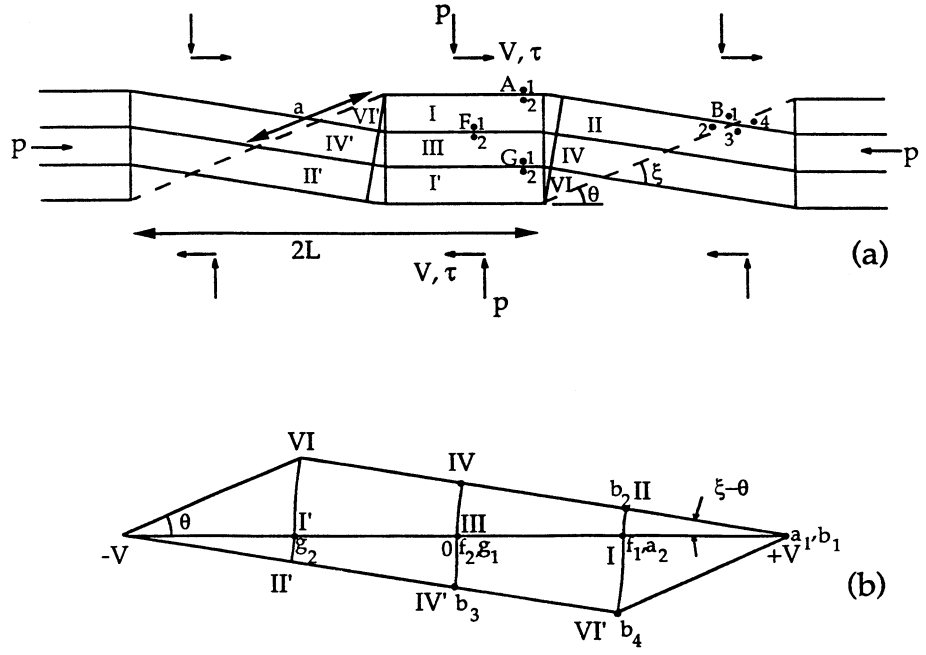

FIG. 5. (a) Slip-line field solution for the integer case $n = 3$ ($\theta \approx 32°$), with $a/L = 2/3$ and crack surface friction coefficient $c = \cos 2\xi$ ($=0$ here). (b) The corresponding hodograph to (a).

The collapse load in shear predicted by the slip-line solution is linearly dependent on a/L,

$$\frac{\tau}{k} = 1 - \frac{a}{L} f(c, \theta_n), \tag{2.3}$$

where

$$f(c, \theta_n) = (1-c)\cos\theta_n - (\cos^{-1} c + \sqrt{1-c^2} - 2\theta_n)\sin\theta_n. \tag{2.4}$$

The remote hydrostatic pressure, p/k, on the crack array and the normal compressive traction t_n/k on the crack surfaces are related by

$$\frac{t_n}{k} = \frac{p}{k} + \left[1 - \frac{a}{L}\cos\theta_n\right](\cos^{-1} c + \sqrt{1-c^2} - 2\theta_n) - \frac{a}{L}(1+c)\sin\theta_n. \tag{2.5}$$

In addition to the restriction imposed by (2.1), the regions of validity for the solution are that (i) $c \leqslant \cos 2\theta$, and (ii) $t_n > 0$, and (iii) $a/L \leqslant 1/\cos\theta$. Equality in the first condition corresponds to "locking up" of the cracks, for which $\tau/k = 1$. The second condition specifies that the cracks may not open up under simple shear deformation. Equality in the final restriction corresponds to the n rigid sliding rectangular blocks shrinking to zero length. In this case, a different slip-line field is needed for more closely spaced cracks.

Although relations (2.3) and (2.5) strictly apply at only the discrete values of θ_n defined by (2.1), these relations provide very good approximations for intermediate values of θ. Figure 6 shows $f(c, \theta)$ as a continuous function of θ for several values of c. The symbols (+), which denote values of θ_n where the simple slip-line fields

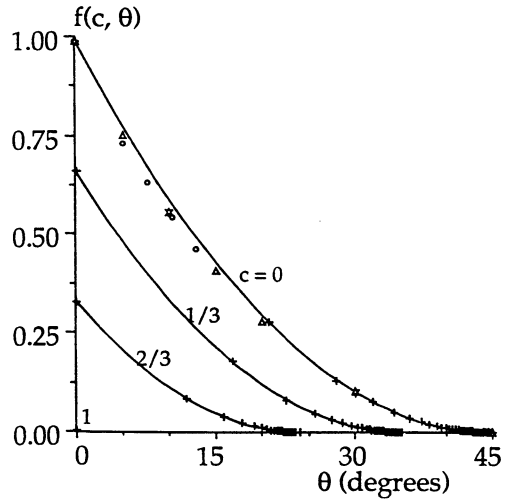

FIG. 6. Slip-line field solution for the nominal collapse load in shear, given by $\tau/k = 1-(a/L)\cdot f(c, \theta)$. Symbols (△) and (▽) denote the finite element predictions for freely sliding cracks with $a/L = 1/3$ and 2/3, respectively. The symbols (+) denote results from the slip-line field solutions at integer values θ_n using (2.1) and (2.4), and symbols (○) denote results for intermediate values of θ as discussed in the Appendix. The smooth curves show the approximate relation obtained by interpreting (2.4) as a continuous function of θ.

described occur, become more closely spaced as the cracks approach the "lock up" orientation $\theta = (\cos^{-1} c)/2$. In this limit, f approaches zero and the material responds as if no cracks are present. More complex slip-line fields for intermediate values of θ between 0 and approximately 15° are briefly presented in the Appendix. The values of $f(c = 0, \theta)$ from the intermediate fields are represented by symbols (○) in Fig. 6, and show relations (2.3) and (2.5) to be good approximations even at lower values of θ where the density of θ_n points is lower. The shear collapse load is therefore a monotonically decreasing function of θ in the range $\theta = 0$ to $(\cos^{-1} c)/2$ and a monotonically increasing function of crack-face friction in the range $c = 0$ to $\cos 2\theta$.

Estimates of $f(c, \theta)$ from the finite element calculations discussed compare favorably with slip-line predictions given by (2.4). In particular, the triangular symbols (△) and (▽) in Fig. 6 show the finite element estimates for friction-free cracks ($c = 0$) of size $a/L = 1/3$ and 2/3, respectively, over an angular range of $\theta = 0$ to 45°. Differences in predictions by the two methods are less than 5%.

The restriction that $t_n > 0$ for the slip-line solution specifies a maximum value of remote hydrostatic tension, $\sigma_m/k = -p/k$, below which the cracks will remain closed. In this case, (2.5) is used to determine σ_m/k by setting $t_n = c = 0$ corresponding to traction-free crack surfaces. Figure 7 shows that σ_m/k is positive over the entire range of a/L and θ. This result indicates important related features of cracked materials. First, substantial crack friction may exist in shear bands, even when hydrostatic tension is present. Further, a simple shear mode of deformation, which involves no macroscopic dilatation, is predicted to persist for the crack array, even though substantial hydrostatic tension may exist. This behavior is not predicted by the Gurson constitutive law for voided materials, since there, void growth is always predicted to accompany local stress states of hydrostatic tension and shear.

The slip-line fields predict that plastic straining occurs in a band of height equal to that of the projected crack height $2a \sin\theta$. This dimension remains constant during collapse of the band in shear. A suitable choice for the average plastic shear strain experienced by the band is

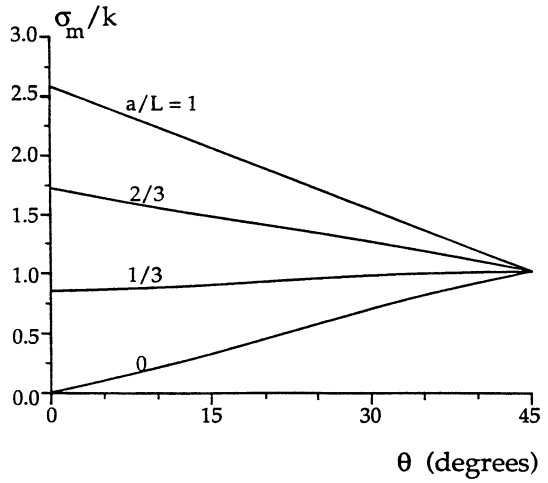

FIG. 7. The maximum value of mean stress, $\sigma_m/k = -p/k$, for which the crack faces in the array under simple shear will remain closed.

$$\gamma^p = U/a \sin\theta, \tag{2.6}$$

where $2U$ is the remote displacement jump across the band.

The hodographs in Figs 4(b) and 5(b) suggest approximate relations to update a/L and θ in terms of the corresponding initial values, denoted by subscript o,

$$\frac{a/L}{(a/L)_o} = \frac{\sin\theta_o}{\sin\theta}, \tag{2.7}$$

$$\cot\theta = \cot\theta_o + \gamma^p. \tag{2.8}$$

The approximation is based on the slip-line prediction that the upper and lower crack tips move at velocity V and $-V$, respectively. The finite element calculations verify this result in the fully plastic range. The above relations also assume that the crack remains straight, rather than kink as the slip-line solution predicts. This seems reasonable for actual materials which work-harden.

An additional result from the hodograph for the crack band in simple shear is the jump, Δv_c, in tangential velocity across the sliding crack surfaces:

$$\Delta v_c = 2V\left[\cos\theta - \sqrt{\frac{1+c}{1-c}}\sin\theta\right]. \tag{2.9}$$

3. The Shear Stress–Strain Response for a Crack Array, Incorporating Strain Hardening

The relation between an increment of loading, $\dot{\tau}$ and an increment of nominal plastic shear strain, $\dot{\gamma}^p$ of the crack array is constructed from the above perfectly plastic analysis. Strain hardening is incorporated approximately by updating the mean flow stress k of the matrix from an initial value k_o.

The incremental stress–strain relation for the crack array is obtained by differentiating (2.3) with respect to time:

$$\frac{\dot{\tau}}{k_o} = \left[1 - \frac{a}{L}f(c,\theta)\right]\frac{\dot{k}}{k_o} - \frac{k}{k_o}\left[f(c,\theta)\left(\frac{a}{L}\right)^{\cdot} + \frac{a}{L}\frac{\partial f}{\partial\theta}\dot{\theta} + \frac{a}{L}\frac{\partial f}{\partial c}\dot{c}\right]. \tag{3.1}$$

Each of the time rates of change on the right side is expressed as a function of $\dot{\gamma}^p$ in order to obtain a relation of the form,

$$\frac{\dot{\tau}}{k_o} = F\dot{\gamma}^p \tag{3.2}$$

where F is the plastic tangent modulus in shear to be determined. The rates of change for crack length and orientation are obtained by differentiating (2.7) and (2.8), respectively,

$$\left(\frac{a}{L}\right)^{\cdot} = \frac{1}{2}\frac{a}{L}\dot{\gamma}^{\mathrm{p}} \sin 2\theta,$$

$$\dot{\theta} = -\dot{\gamma}^{\mathrm{p}} \sin^2 \theta. \tag{3.3}$$

The current flow stress of the matrix varies spatially within the band, due to nonuniform straining caused by the cracks. The formulation in (3.1) is therefore approximate in that an average value, $\bar{k}$, for the flow stress in shear must be assigned. The rate of change, $\dot{\bar{k}}$, is determined by equating the external plastic work rate performed on the crack array to that dissipated internally. If $\dot{w}(\mathbf{x}) = \sigma_{ij}\dot{\varepsilon}^{\mathrm{p}}_{ij}$ is the rate of internal dissipation in a unit element of matrix at position $\mathbf{x}$, the equivalence of internal and external plastic work is written as

$$2(\tau \cdot V \cdot 2L) - t_{\mathrm{s}} \cdot \Delta v_{\mathrm{c}} \cdot 2a = \int_A \dot{w}(\mathbf{x})\, \mathrm{d}\mathbf{x}, \tag{3.4}$$

where $A = 2L \cdot 2a \sin\theta$ denotes the area of integration over a periodic cell of the crack array.

The right side of (3.4) can be evaluated in terms of an average plastic energy dissipation rate, $\dot{\bar{w}}$, per unit volume of matrix times A. In the case of a hardening matrix described by J_2 theory, the dissipation rate is

$$\dot{w}(\mathbf{x}) = \frac{\sigma_{\mathrm{e}}(\mathbf{x})}{h(\sigma_{\mathrm{e}})}\dot{\sigma}_{\mathrm{e}}(\mathbf{x}), \tag{3.5}$$

where $\sigma_{\mathrm{e}}(\mathbf{x}) = \sqrt{3}k(\mathbf{x})$ is the effective flow stress, and $h(\sigma_{\mathrm{e}}) = \mathrm{d}\sigma_{\mathrm{e}}/\mathrm{d}\varepsilon^{\mathrm{p}}_{\mathrm{e}}$ is the slope of the effective stress–plastic strain curve. An average value, $\dot{\bar{k}}$, in the band is defined from the above relation by

$$\dot{\bar{w}} = 3\bar{k}\dot{\bar{k}}/h(\sqrt{3}\bar{k}). \tag{3.6}$$

Using relations (2.2), (2.9) and (3.4)–(3.6), an average rate of change of flow stress is given as

$$\frac{\dot{\bar{k}}}{k_{\mathrm{o}}} = \frac{1}{3}\frac{h}{k_{\mathrm{o}}}\dot{\gamma}^{\mathrm{p}}\left[\frac{\tau}{\bar{k}} - \frac{a}{L}c\left(\cos\theta - \sqrt{\frac{1+c}{1-c}}\sin\theta\right)\right]. \tag{3.7}$$

The slope $h = h(\sqrt{3}\bar{k})$ of the effective stress–plastic strain curve represents the only input of the mechanical response of the matrix. For the particular case where the matrix follows a power-law relation in shear described by

$$\frac{\tau_{\mathrm{m}}}{k_{\mathrm{o}}} = \begin{cases} \gamma_{\mathrm{m}}/\gamma_{\mathrm{y}} & (\text{elastic range, } \tau_{\mathrm{m}}/k_{\mathrm{o}} \leqslant 1) \\ (\gamma_{\mathrm{m}}/\gamma_{\mathrm{y}})^{N} & (\text{elastic–plastic range, } \tau_{\mathrm{m}}/k_{\mathrm{o}} > 1) \end{cases}, \tag{3.8}$$

the slope h is defined in terms of the elastic and tangent moduli G, G_{t} according to

$$\frac{1}{h} = \frac{1}{3}\left(\frac{1}{G_{\mathrm{t}}} - \frac{1}{G}\right), \quad G_{\mathrm{t}} = \frac{\mathrm{d}\tau_{\mathrm{m}}}{\mathrm{d}\gamma_{\mathrm{m}}} = NG\left(\frac{\tau}{k_{\mathrm{o}}}\right)^{(N-1)/N}. \tag{3.9}$$

The rate of change $\dot{c}$ of the crack-face friction coefficient depends, in general, on

the material surface roughness, lubrication and traction t_n normal to the crack surface. The work of WANHEIM *et al.* (1978, 1980) indicates that c may be approximated as independent of t_n at very small and at very large values of t_n. Under these conditions and also in the case of freely sliding boundaries where $c = 0$, it may be reasonable to assume $\dot{c} = 0$. In intermediate cases where frictional properties may be more accurately described by a constant coefficient of friction $\mu = t_s/t_n$, (2.5) may be used to obtain an explicit relation for $\dot{c}$ under conditions of constant remote pressure p:

$$\dot{c} = \mu\left[-\frac{ph}{3\bar{k}^2}\left\{\frac{\tau}{\bar{k}} - \frac{a}{L}c\left(\cos\theta + \sqrt{\frac{1+c}{1-c}}\sin\theta\right)\right\} - 2\sin^2\theta\cos 2\theta\right]\dot{\gamma}^p \Big/ \left(1 + \frac{\mu}{\sqrt{1-c^2}}\right). \quad (3.10)$$

The plastic tangent modulus F defined in (3.2) may be determined from substitution of (3.3), (3.7) and (3.10) for the rates of change of $(a/L)^{\cdot}$, $\dot{\theta}$, $\dot{\bar{k}}$ and $\dot{c}$ into (3.1). Approximating the elastic shear modulus of the crack array as G, the incremental shear stress–strain relation is written as

$$\frac{\dot{\tau}}{k_o} = \left(\frac{1}{G} + \frac{1}{F}\right)^{-1}\dot{\gamma}. \quad (3.11)$$

Although F and G are comparable at low strains, $1/G \ll 1/F$ at larger strains, and therefore, can be ignored.

Figure 8(a–d) shows the shear stress–strain curves obtained from numerical integration of (3.11) to very large values of shear strain. In all cases, the crack-face friction coefficient is assumed to be constant. Some prominent features are the initial increase in nominal shear stress produced by work hardening of the matrix, and the development of a maximum in τ corresponding to $F = 0$, beyond which softening mechanisms of crack growth and rotation dominate over work hardening. Each of the curves requires an initial geometry described by $(a/L)_o$ and θ_o. Figure 8(a) shows that the maximum τ and the corresponding shear strain at which it occurs increase with matrix hardening exponent. Figure 8(b) indicates that the critical value of τ at which $F = 0$ increases between 0 and 45° with decreasing initial crack angle θ_o. As θ approaches 0, the work hardening rate increases due to a decrease in both the volume of material contained in the band and the rate of crack stretching and rotation. Figure 8(c) displays the reduction in the maximum value of τ and corresponding value of shear strain due to a higher initial crack length to spacing ratio $(a/L)_o$. Figure 8(d) demonstrates the increase in the maximum value of τ and the corresponding value of shear strain which accompany higher crack-face friction.

The approximations involved in incorporating work hardening were tested by comparing shear stress–strain curves predicted by (3.11) to those calculated from FEM studies which incorporate a power-law behavior for the matrix as described in (3.8). Figure 9 shows predicted curves for the case of $\theta_o = 30°$, $(a/L)_o = 2/3$, $N = 0.1$ and $\gamma_y = 10^{-3}$; the agreement is good. This supports the approximation made earlier

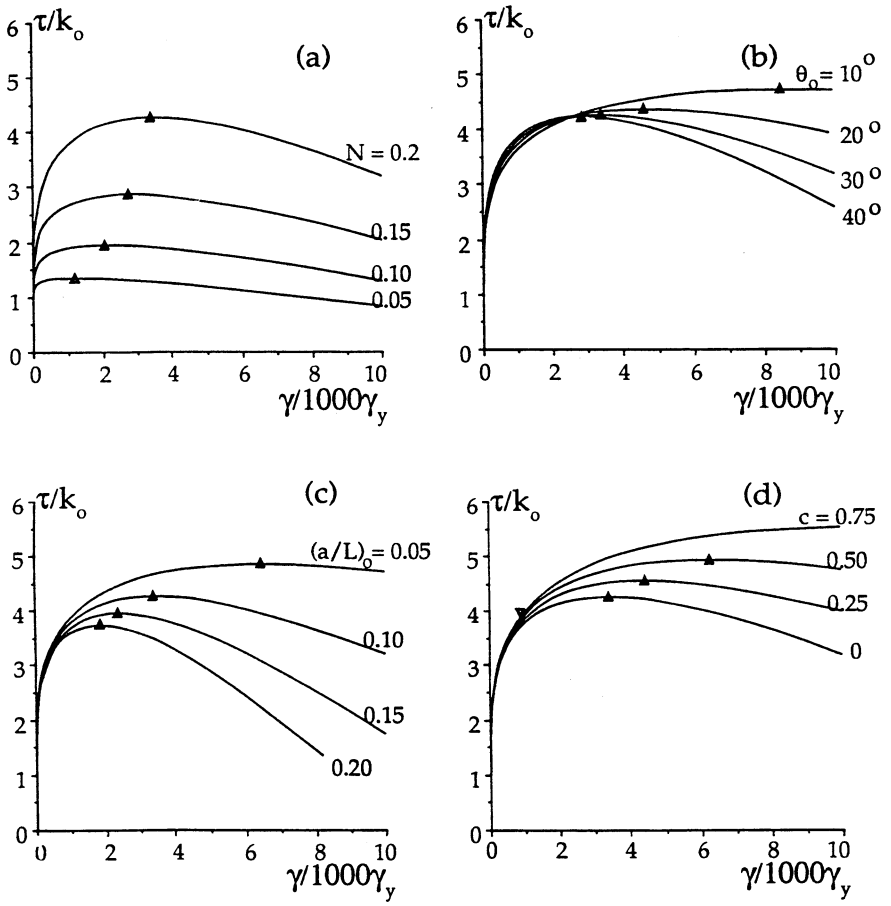

FIG. 8. Shear stress–strain curves for a cracked material (a) as a function of matrix hardening exponent N, using initial values of $\theta_o = 30°$, $(a/L)_o = 0.1$ and $c = 0$, (b) as a function of initial crack orientation angle θ_o using $N = 0.2$, $(a/L)_o = 0.1$ and $c = 0$, (c) as a function of the initial ratio $(a/L)_o$ of crack length to crack spacing, using $N = 0.2$, $\theta_o = 30°$ and $c = 0$, and (d) as a function of crack surface friction coefficient c, using $N = 0.2$, $\theta_o = 30°$ and $(a/L)_o = 0.1$. The symbol (▲) indicates where the maximum shear stress occurs on each curve, and (▼) indicates a transition from locked to unlocked crack sliding conditions for the case $c = 0.75$.

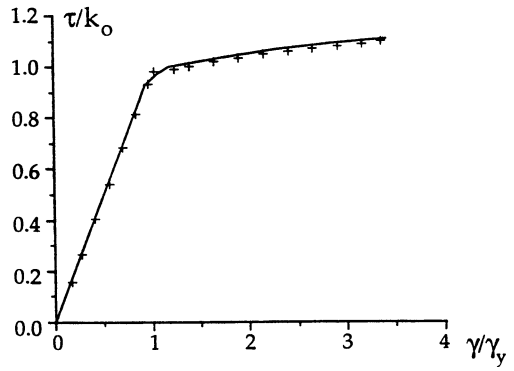

FIG. 9. Comparison of shear stress–shear strain results predicted by the approximate slip-line field model incorporating strain hardening (solid line) to finite element results (+), for the case of $(a/L)_o = 2/3$, $\theta_o = 30°$, yield strain in shear $\gamma_y = 0.001$, and power-law hardening exponent $N = 0.1$.

to characterize the work hardening rate in terms of an average value of flow stress, even though spatial variations exist in the band.

4. Estimates of Ductility Due to Shear Localization

A simple model of shear ductility is depicted in Fig. 10, where a body is loaded under simple shear and the incipient shear band containing cracks is bounded by uncracked material on either side of it and is oriented parallel to the shearing direction. The crack band is assumed to obey the shear stress–strain relation developed in Section 3 for an array of inclined cracks surrounded by a power-law matrix, and the uncracked "external" material obeys the relation for the matrix. The band and external material each deform by simple shear, and the critical condition for localization is stated as $\dot{\gamma}_{\text{band}}/\dot{\gamma}_{\text{external}} \to \infty$. This occurs when the modulus F of the band (see (3.11)) approaches zero, or equivalently, when a peak stress τ_{loc}/k_o is reached in the band. At this point, the external material is sustaining a load τ_{loc}/k_o, and has strained a corresponding amount $\gamma_{\text{loc}}/\gamma_y$ given by (3.8).

If the band is negligibly thin compared to the specimen height, as shown in Fig. 10, $\gamma_{\text{loc}}/\gamma_y$ will define the localization strain. The highly deforming band is assumed to fracture upon localization by crack linkage, and $\gamma_{\text{loc}}/\gamma_y$ may therefore be a measure of the ductility of the material in simple shear.

Figure 11(a, b) displays for $c = 0$ and $c = 0.5$, respectively, $\gamma_{\text{loc}}/\gamma_y$ as a function of the initial crack length and crack orientation in the band. In each case, the ductility is found to decrease with increasing initial crack length. This is supported by results in Fig. 8(c), where the peak nominal shear stress is observed to decrease with increasing initial crack length. Comparison of Fig. 11(a, b) shows an increase in strain to localization with crack-face friction factor c. This is consistent with the increase in peak nominal shear stress with c in Fig. 8(d). The effect of hardening, although not shown in Fig. 11, is clearly observed in Fig. 8(a). Here, an increase in matrix hardening exponent N strongly increases the peak nominal shear stress, and the strain to localization.

The dependence of localization strain on initial angle θ_o is more complex. As θ_o approaches 45°, (2.3) and (2.4) show that τ_o/k approaches 1 and the initial rate of

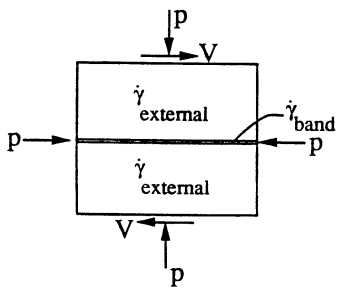

FIG. 10. A model for localization in simple shear, in which the incipient shear 'band' is assumed to contain an initial imperfection modelled as a band of cracks, and the surrounding, 'external' material is assumed to be uncracked.

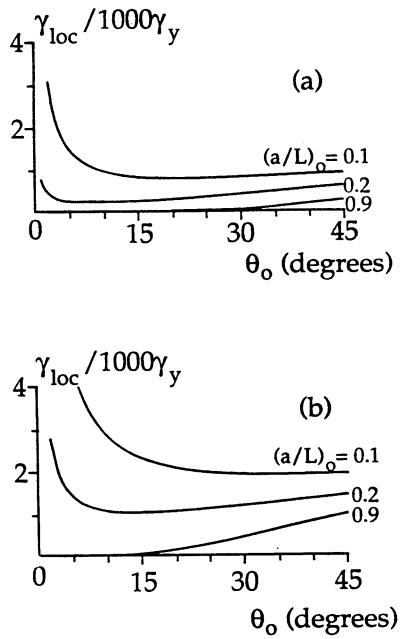

FIG. 11. Prediction of the strain to localization, γ_{loc}/γ_y, as a function of the initial crack orientation angle θ_o and initial crack length to spacing ratio $(a/L)_o$ for (a) $c = 0$ (friction-free cracks) and (b) $c = 0.5$ (frictional cracks produced by the confining pressure p). In each case, $\gamma_y = 0.001$ and $N = 0.1$.

plastic work in the band and external material become equal. As θ_o and $(a/L)_o$ approach 0, the small volume of material in the very thin crack band rapidly work-hardens. These two features account for the general increase in ductility seen in Fig. 11 as θ_o approaches 45°, and as $(a/L)_o$ and θ_o approach 0. In the limit as θ approaches 0, there are no softening mechanisms to cause the incremental shear modulus in the band to reach zero, and the localization strain is predicted to be unbounded.

The prediction of unbounded localization strain as θ_o approaches 0 suggests important additional softening mechanisms to those modelled. In particular, additional cracks may nucleate in the highly deforming ligaments between original cracks. Further, the localization analysis presented restricts the imperfection band to be parallel to the simple shear direction, and precludes additional softening due to the rotation and stretching of the entire imperfection band. These softening mechanisms require further information on crack nucleation criteria, such as that used by SAJE *et al.* (1982) for localization due to void softening, and also on the constitutive relation for crack bands in deformation modes other than simple shear. The analysis also neglects crack tip growth as a softening mechanism. Little appears to be known about crack tip growth laws in plastic shear fields. As such, the strains to localization presented should be regarded as upper bounds.

5. CONCLUSIONS

Flow localization in shear has been shown to occur in materials containing an initial imperfection of cracks. The localization occurs because the damage evolution in

shear, modelled here by crack rotation and stretching, can substantially reduce the incremental stiffness of the material to a point of mechanical instability, even when strain hardening is present. The strain to localization is found to depend on initial crack orientation angle, crack size to spacing ratio, crack-face friction and material work-hardening. The strong dependence of localization strain on the initial crack orientation relative to the shearing direction demonstrates the important effect that anisotropy of damage may have in localization phenomena. This may be present under applied deformations such as simple shear, in which the material anisotropy, represented here by cracking, rotates relative to the loading axes.

Results for localization of deformation in a cracked band may be useful when confining pressures suppress void growth. A particular example is the delamination wear of materials under sliding frictional contact, in which the nucleation and growth of near-surface cracks is thought to initiate shear localization and the production of wear flakes, SUH (1986). Further, the inclusion of crack-face friction in the model developed may be useful in understanding the pressure dependence of ductile fracture in shear, as noted by TEIRLINK *et al.* (1988). In the present model, the strain to localization in shear is predicted to increase with crack-face friction until locking of the crack faces occurs.

ACKNOWLEDGEMENTS

The work of P. M. ANDERSON was sponsored in part by SERC and in part by the American Association of Railroads. Stimulating discussions with I. F. COLLINS are greatly appreciated.

REFERENCES

DEWHURST, P. and COLLINS, I. F. 1973 *Int. J. Num. Meth. Engng* **7**, 357.

GREEN, A. P. 1954 *J. Mech. Phys. Solids* **2**, 197.

GURSON, A. L. 1975 Ph.D. Thesis, Brown University.

GURSON, A. L. 1977 *J. Engng Mater. Tech. Trans. ASME* **99**, 2.

KAPOOR, A. J. 1987 Ph.D. Thesis, University of Cambridge.

MARC 1983 Users Manual, Version K 1.3, MARC Analysis Research Corporation.

NAGPAL, V., MCCLINTOCK, F. A., BERG, C. A. and SUBUDHI, M. 1972 In *Int. Symp. on Foundations of Plasticity* (edited by A. SAWCZUK), Vol. 1, p. 365. Noordhoff, Leyden.

NAGTEGAAL, J. C., PARKS, M. and RICE, J. R. 1974 *Comput. Meth. Appl. Mech. Engng* **4**, D.153.

SAJE, M., PAN, J. and NEEDLEMAN, A. 1982 *Int. J. Fracture* **19**, 163.

SUH, N. P. 1986 *Tribophysics*, Prentice-Hall, London.

TEIRLINK, D., ZOK, F., EMBURY, J. D. and ASHBY, M. F. 1988 *Acta Metall.* **36**, 1213.

WANHEIM, T. and ABILDGAARD, T. 1980 *Proc. 4th Int. Conf. on Production Engng*, Tokyo, p. 122. The Japan Society for Technology of Plasticity, Tokyo.

WANHEIM, T. and BAY, N. 1978 *Ann. CIRP* **27**, 1.

YAMAMOTO, H. 1978 *Int. J. Fracture* **14**, 347.

APPENDIX

Slip-line fields of simple type exist for crack inclination angles θ less than approximately 15°. These fields are similar to those proposed by GREEN (1954) for surface asperity contacts. Typical fields are given in Fig. A1 for $\theta = 5°$, $a/L = 0.5$ and friction factor $c = 0$ and 0.5. The fields consist of a circular fan with straight radial slip lines emanating from each crack tip. The circular fan is adjacent to a singular fan with curved boundaries at the neighboring crack tip. Unlike the slip-line fields of integer n described in the body of the paper, the plastic regions adjacent to the crack faces are zones which deform under non-constant stress. In a manner

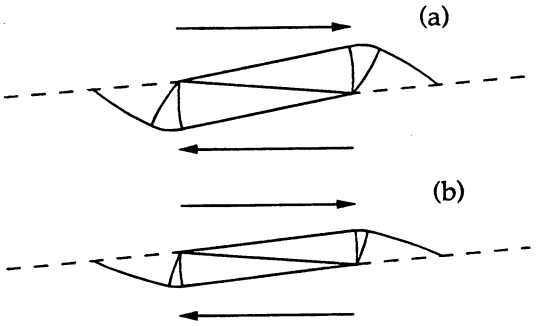

FIG. A1. The slip-line fields for crack arrays in shear as shown in Fig. 2, with $\theta = 5°$, $a/L = 0.5$ and crack-face friction coefficient (a) $c = 0$ and (b) $c = 0.5$.

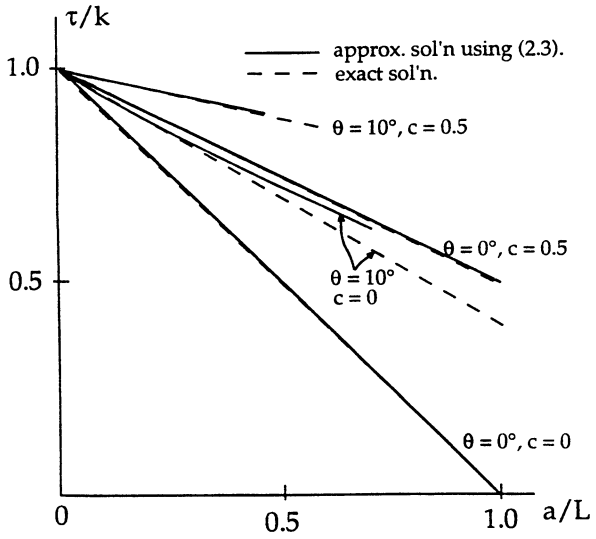

FIG. A2. The nominal shear collapse load τ for an array of cracks as shown in Fig. 2(a), as given by the exact solution (——) and approximate solution (– – – –) obtained by interpreting (2.3) as a continuous function of θ. k is the flow stress of the matrix, a/L is the crack length to spacing ratio and θ is the crack orientation angle.

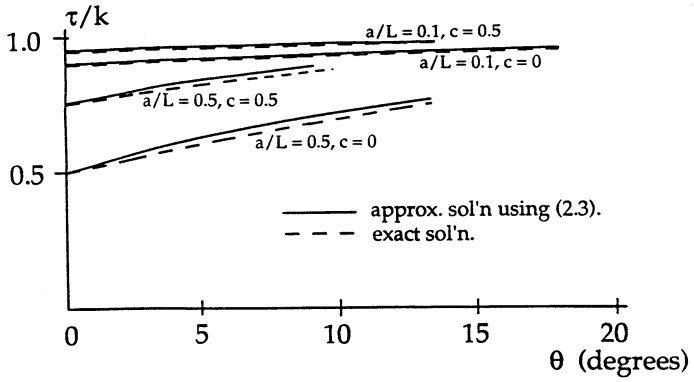

FIG. A3. The nominal shear collapse load τ for an array of cracks as shown in Fig. 2(a), as given by the exact solution (——) and approximate solution (– – – –) obtained by interpreting (2.3) as a continuous function of θ. k is the flow stress of the matrix, a/L is the crack length to spacing ratio and θ is the crack orientation angle.

similar to the $n = 1$ solution given in Fig. 4, the crack kinks at its midpoint due to a line of velocity discontinuity that intersects the crack.

The slip-line fields presented here were constructed using the matrix method developed by DEWHURST and COLLINS (1973). The main shear traction τ carried by the crack array is shown in Fig. A2 as a function of a/L for selected angles θ, and in Fig. A3 as a function of θ for selected a/L. These figures show that the analytic approximation in which (2.3) and (2.4) are treated as continuous functions of θ agrees with the exact fields to within 3%. Further, the shear traction τ carried by the band decreases almost linearly with increasing a/L, as predicted by (2.3). We conclude that the analytic approximation using (2.3) and (2.4) is satisfactory for our purposes. It is exact for all discrete values of θ_n between 0° and 45° given by (2.1).

The simple fields given in Fig. A1 are not valid for θ larger than approximately 15°; at larger θ values, negative plastic work is predicted on the slip line of velocity discontinuity joining neighboring crack tips. The domain of validity of the simple fields is given in Figs A2 and A3.